Non-innocent intercalation of diamines into tetragonal FeS superconductor

Colin P. Harmer, a,b Chongin Pak, Joshua T. Greenfield, Adedovin N. Adeyemi, Eranga H.

Gamage, a,b Kirill Kovnir a,b,\*

<sup>a</sup> Department of Chemistry, Iowa State University, Ames, Iowa 50011, USA

<sup>b</sup> Ames Laboratory, U.S. Department of Energy, Ames, Iowa 50011, USA

<sup>c</sup> Department of Chemistry, University of California, Davis, Davis, CA 95616, USA

**ABSTRACT** 

We report solvothermal pathways towards intercalated iron-sulfide, two

 $[Fe_8S_{10}]Fe(en)_3 \cdot en_{0.5}$  (en = ethylenediamine), featuring  $[Fe_8S_{10}]^{2-}$  layers stacked by  $[Fe(en)_3]^{2+}$ 

cations and free ethylenediamine molecules. [Fe<sub>8</sub>S<sub>10</sub>]Fe(en)<sub>3</sub>·en<sub>0.5</sub> is synthesized in a simple

single-step method from Fe and S in ethylenediamine with addition of NH<sub>4</sub>Cl mineralizer as well

as from solvothermal treatment of mackinawite, tetragonal FeS. *In situ* synchrotron powder X-ray

diffraction experiments reveal a clear transformation of tetragonal FeS into [Fe<sub>8</sub>S<sub>10</sub>]Fe(en)<sub>3</sub>·en<sub>0.5</sub>

upon reaction with ethylenediamine. In-house control synthetic experiments confirmed the

chemical process, whereby ethylenediamine leaches iron solely from the tetragonal Fe-S layers to

form [Fe(en)<sub>3</sub>]<sup>2+</sup> complexes and thereby oxidizing the intralayer iron to Fe<sup>2.25+</sup>. Our report

emphasizes that, in layered iron-chalcogenides, diamines can intercalate as charged coordination

complexes in tandem with neutral diamine molecules.

**KEYWORDS:** iron chalcogenide, solvothermal synthesis, intercalation, crystal structure, in-situ

1

#### INTRODUCTION

Intercalation into tetragonal iron chalcogenides has been of high interest to understand the interplay of superconductivity and magnetism with structural and compositional variations. The parent compounds, tetragonal iron sulfide (mackinawite FeS) and selenide (β-FeSe), exhibit superconductivity below 5 K and 8 K, respectively.<sup>1-4</sup> In these parent compounds iron atoms are arranged in a square net, tetrahedrally coordinated by a chalcogen (Ch) atoms to make neutral Fe-Ch layers. The layers are stacked via van der Waals interactions making them ideal candidates for intercalation.<sup>5</sup> As such, a variety of novel intercalates such as alkali metal hydroxides,<sup>6</sup> alkali metal amides,<sup>7</sup> and diamines<sup>8-10</sup> have been reported to enhance the superconductivity onset (T<sub>c</sub>) up to 45 K.<sup>5</sup>

Intercalation from liquid ammonia as well as hydrothermal intercalation of alkali hydroxides have produced notable structures. Numerous studies on Li<sub>0.6</sub>(NH<sub>2</sub>)<sub>y</sub>(NH<sub>3</sub>)<sub>1-y</sub>Fe<sub>2</sub>Se<sub>2</sub> showed ammonia could facilitate alkali metal insertion, and could also participate in the intercalation itself as both a molecular spacer and in reacting to form LiNH<sub>2</sub> units.<sup>7, 11-12</sup> In the case of the (LiOH)FeSe system, it was shown that intercalation can result in antisite defects where Li and Fe can be interchanged in the hydroxide layer.<sup>6, 13</sup>

The current report describes a dual-role diamine intercalate of the simplest example, ethylenediamine. We demonstrate its ability to intercalate as free ligand and as coordinating species analogous to the liquid ammonia system, as well as its ability to extract iron from the FeCh layer into the interlayer space like the LiOH system.

While van der Waals stacking allows for a variety of intercalates, full structural characterization of the intercalation products is a challenge due to weak interlayer interactions, often resulting in a high degree of twinning, stacking faults, and gradients of intercalate concentration. This leads to low crystal quality and substantial non-uniform broadening of the

diffraction peaks. As such many reports have had to rely on refinement of moderate quality powder diffraction data to model the crystal structure. 8-9, 14-15 Intercalations with diamines can increase the complexity for modeling. The structure within the Fe-Ch layers, composed of the strongest X-ray scatterers in the compound, can generally be modeled with a high degree of confidence because of its inherent rigidity and regularity. The intercalates on the other hand are made up of weakly scattering lighter atoms (C, N, and H), which makes the intercalates composition and structure contributions near negligible towards diffraction peak intensities and refinement statistics. In the case of ammonia intercalation, neutron diffraction proved crucial to fully determine the structure. Thowever, deuteration of diamine samples is extremely cost prohibitive. For example, this report features [Fe<sub>8</sub>S<sub>10</sub>]Fe(en)<sub>3</sub>·en<sub>0.5</sub> which would cost over \$200,000 in commercial sources of deuterated d<sub>8</sub>-ethylenediamine to synthesize enough sample for a neutron powder diffraction experiment.

Furthermore, diamine intercalates demonstrate a high degree of structural flexibility due to the reactivity of diamines, which have a high propensity to chelate transition metals, including Fe. 16-17 This propensity for iron can not only leach Fe from the Fe-Ch layers but also produce *in situ* new intercalating species, Fe-diamine chelation complexes. Iron migration from Fe-Ch layers to the interlayer space adds a particular challenge when finding the composition by spectroscopic methods like energy dispersive X-ray spectroscopy. Even when disregarding potential depletion of crystals with chalcogen upon electron irradiation, an experimentally observed ratio of Fe to Ch as Fe<sub>1</sub>Ch<sub>1</sub> may actually correspond to an Fe-vacancy layer combined with Fe-intercalate, [Fe<sub>1-x</sub>Ch][Fe<sub>x</sub>(diamine)].

We focused on the simplest diamine intercalation system, Fe-S-en, (en = ethylenediamine). This report details the synthetic method and complex crystal structure of  $[Fe_8S_{10}]Fe(en)_3 \cdot en_{0.5}$  and

demonstrates how this compound can be formed *in situ* by the reaction of tetragonal FeS and en. We have chosen to highlight [Fe<sub>8</sub>S<sub>10</sub>]Fe(en)<sub>3</sub>·en<sub>0.5</sub> because it brings up crucial aspects of diamine intercalated iron-chalcogenides. Our report shows that ethylenediamine can not only intercalate between Fe-S layers as a free ligand and as an iron-diamine coordination complex in the same compound but also can *in situ* leach Fe from the tetragonal Fe-S layers.

### **RESULTS & DISCUSSION**

[Fe<sub>8</sub>S<sub>10</sub>]Fe(en)<sub>3</sub>·en<sub>0.5</sub> was first reported by *Jing Li et al.* in 2010.<sup>18</sup> Single crystal X-ray diffraction from our sample confirms it crystallizes in the monoclinic space group  $P2_1/c$  (No. 14) and is composed of [Fe<sub>8</sub>S<sub>10</sub>]<sup>2-</sup> square tetrahedral layers intercalated by [Fe(en)<sub>3</sub>]<sup>2+</sup> octahedral complexes as well as free ethylenediamine molecules (a = 8.3633(5) Å, b = 33.225(2) Å, c = 20.543(1) Å,  $β = 90.111(1)^\circ$ ). The average Fe–N distance of 2.22(2) Å indicates a high spin Fe<sup>2+</sup> ion in the [Fe(en)<sub>3</sub>]<sup>2+</sup> octahedral complex.<sup>16,19</sup> The layers themselves are like those in mackinawite FeS, but with one fifth of the sites vacant in an ordered motif (**Figure 1**), resulting in a  $\sqrt{5} \times 4\sqrt{5}$  superstructure in the plane of the Fe-S layer and a ca. 5.2 Å increase in the interlayer spacing. The vacancies originate to partially balance the charge of the intercalated [Fe(en)<sub>3</sub>]<sup>2+</sup> species. In mackinawite iron atoms form a perfect square net on the (001) plane, whereas in [Fe<sub>8</sub>S<sub>10</sub>]Fe(en)<sub>3</sub>·en<sub>0.5</sub> they form a puckered sheet due to the Fe atoms displacement by 0.5 Å from the (001) plane. The ordered vacancies and puckered layers result in the distortion of the FeS<sub>4</sub> tetrahedra with ∠S-Fe-S ranging 99-123°. [Fe(en)<sub>3</sub>]<sup>2+</sup> octahedra of the same chirality intercalate each layer leading to alternating planes of Λ and Δ isomers in ABAB fashion.

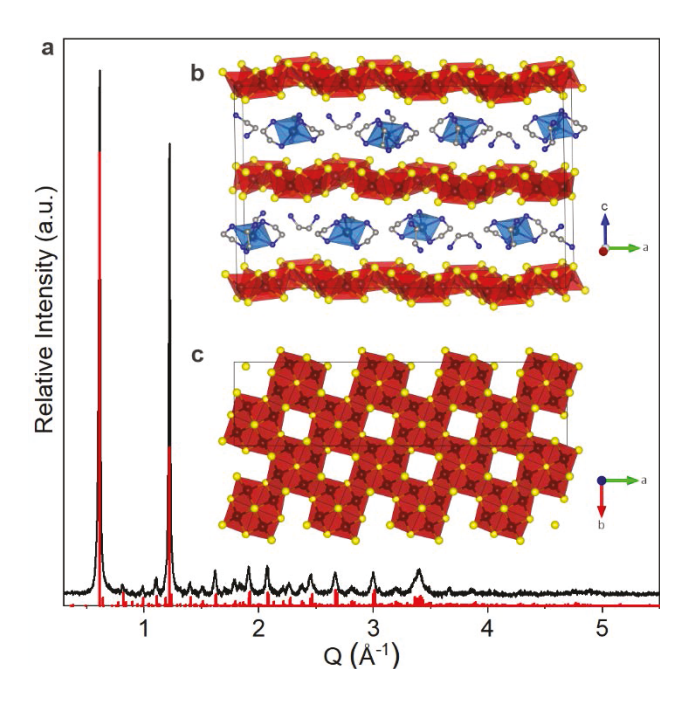


**Figure 1. (a)** Laboratory PXRD pattern (Cu- $K_{\alpha}$ ) of [Fe<sub>8</sub>S<sub>10</sub>]Fe(en)<sub>3</sub>·en<sub>0.5</sub> in black plotted with red ticks indicating peak positions for calculated pattern based on the structural model. **(b)** Crystal structure of [Fe<sub>8</sub>S<sub>10</sub>]Fe(en)<sub>3</sub>en<sub>0.5</sub> with hydrogen atoms omitted for clarity **(c)** Top view of [Fe<sub>8</sub>S<sub>10</sub>]<sup>2-</sup> layers. FeS<sub>4</sub>: red tetrahedra; [Fe(en)<sub>3</sub>]<sup>2+</sup>: blue octahedra; Fe: black; S: yellow; C: grey; N: blue.

Formation of Fe vacancies is common for FeCh intercalated phases, such as  $A_2$ Fe<sub>4</sub>Ch<sub>5</sub> (A = alkali metal) phases, which similar to [Fe<sub>8</sub>S<sub>10</sub>]Fe(en)<sub>3</sub>·en<sub>0.5</sub> possess 20% iron vacancies in the Fe-Ch layer.<sup>20-21</sup> Such vacancies are ordered, as demonstrated by single crystal diffraction,<sup>22</sup> in a motif analogous to the Fe-S layers in [Fe<sub>8</sub>S<sub>10</sub>]Fe(en)<sub>3</sub>·en<sub>0.5</sub>. Vacancies in the Fe-Ch layers resulted in the loss of superconducting properties and development of antiferromagnetism in A<sub>2</sub>Fe<sub>4</sub>Ch<sub>5</sub>.<sup>21-26</sup> Similarly, our studies show that [Fe<sub>8</sub>S<sub>10</sub>]Fe(en)<sub>3</sub>·en<sub>0.5</sub> is a paramagnet with antiferromagnetic nearest-neighbor interactions (**Figure S1**). Optical measurements reveal a weak adsorption feature at 0.58(3) eV which may correspond to the bandgap (**Figure S2**). Similar bandgap range of 0.6-0.8 eV was reported previously for this compound.<sup>18</sup>

[Fe<sub>8</sub>S<sub>10</sub>]Fe(en)<sub>3</sub>en<sub>0.5</sub> was synthesized via a solvothermal method by combining elemental iron and sulfur powders in ethylenediamine used as both solvent and reagent, with the addition of ammonium chloride as a mineralizer. This highly reproducible synthesis produces [Fe<sub>8</sub>S<sub>10</sub>]Fe(en)<sub>3</sub>·en<sub>0.5</sub> as dark brown platelets, *ca.* 0.5 x 0.5 x 0.001 mm<sup>3</sup>, and a byproduct of Fe(en)<sub>3</sub>Cl<sub>2</sub> as white chunks. Subsequent washing with ethanol leaves clean [Fe<sub>8</sub>S<sub>10</sub>]Fe(en)<sub>3</sub>·en<sub>0.5</sub>, as determined by benchtop powder X-ray diffraction (PXRD). Further characterization by high resolution synchrotron PXRD verified sample homogeneity (**Figure S3**). Thermal gravimetric analysis shows the as prepared sample is stable up to 200 °C, at which point, a significant weight loss is observed indicating decomposition. Details of the synthetic methods and synchrotron PXRD analysis are provided in the **SI**.

Based on our synthetic attempts we hypothesized that ethylenediamine can *in situ* leach Fe from Fe-S layers of mackinawite leading to an oxidation of intralayer iron form Fe<sup>2+</sup> in neutral FeS layers to Fe<sup>2.25+</sup> in [Fe<sub>8</sub>S<sub>10</sub>]<sup>2-</sup> layers. The precursor, mackinawite, was prepared solvothermally from Fe and S in dimethylformamide at 150 °C for one day. PXRD analysis of the products reveals a black powder with mackinawite, tetragonal FeS, as the major phase along with admixtures of hexagonal Fe<sub>1-x</sub>S and elemental Fe. Solvothermal treatment of that mixture with excess of ethylenediamine in presence of NH<sub>4</sub>Cl mineralizer yielded [Fe<sub>8</sub>S<sub>10</sub>]Fe(en)<sub>3</sub>·en<sub>0.5</sub>. As opposed to the synthesis from elements, where [Fe<sub>8</sub>S<sub>10</sub>]Fe(en)<sub>3</sub>·en<sub>0.5</sub> crystals grew as large platelets, synthesis from mackinawite resulted in a fine black powder indicating that transformation of finely ground mackinawite to [Fe<sub>8</sub>S<sub>10</sub>]Fe(en)<sub>3</sub>·en<sub>0.5</sub> is topotactic.

In situ synchrotron PXRD experiments conducted at beamline 17-BM-B at the Advanced Photon Source at Argonne National Laboratory were used to further investigate the structural transformation from FeS (mackinawite) to [Fe<sub>8</sub>S<sub>10</sub>]Fe(en)<sub>3</sub>·en<sub>0.5</sub>. Full details of the *in situ* 

synchrotron PXRD setup specific to solvothermal samples are described elsewhere. A few milligrams of FeS starting material were added to a silica capillary which was subsequently filled with ethylenediamine and pressurized with He to simulate solvothermal conditions. The sample was then heated from 25 °C to 240 °C with a hot air blower at a constant rate of 3 °C/min. For cooling, heaters were switched off and data was collected until the sample reached 30 °C.

As shown in **Figure 2**, FeS (mackinawite), and minor amounts of Fe<sub>1-x</sub>S (hexagonal) and elemental Fe are the starting materials. At about 70 °C a new peak begins to form at 0.6 Å<sup>-1</sup> ( $d \sim 10.4$  Å) concurrent with shifting of the peak at 1.25 Å<sup>-1</sup> to 1.21 Å<sup>-1</sup> ( $d \sim 5.2$  Å), corresponding to the most intense (002) and (004) peaks of [Fe<sub>8</sub>S<sub>10</sub>]Fe(en)<sub>3</sub>·en<sub>0.5</sub>. As the sample is heated, [Fe<sub>8</sub>S<sub>10</sub>]Fe(en)<sub>3</sub>·en<sub>0.5</sub> peaks continue to grow along with a commensurate loss of intensity of mackinawite peaks. Beyond 210 °C there is no further evidence of crystalline mackinawite. [Fe<sub>8</sub>S<sub>10</sub>]Fe(en)<sub>3</sub>·en<sub>0.5</sub> peaks continue to sharpen as the sample reaches 240 °C. No substantial transformations, besides temperature-induced unit cell contraction, are observed upon cooling. The final pattern shows [Fe<sub>8</sub>S<sub>10</sub>]Fe(en)<sub>3</sub>·en<sub>0.5</sub> as the major phase with Fe<sub>1-x</sub>S (hexagonal) and elemental Fe remaining.

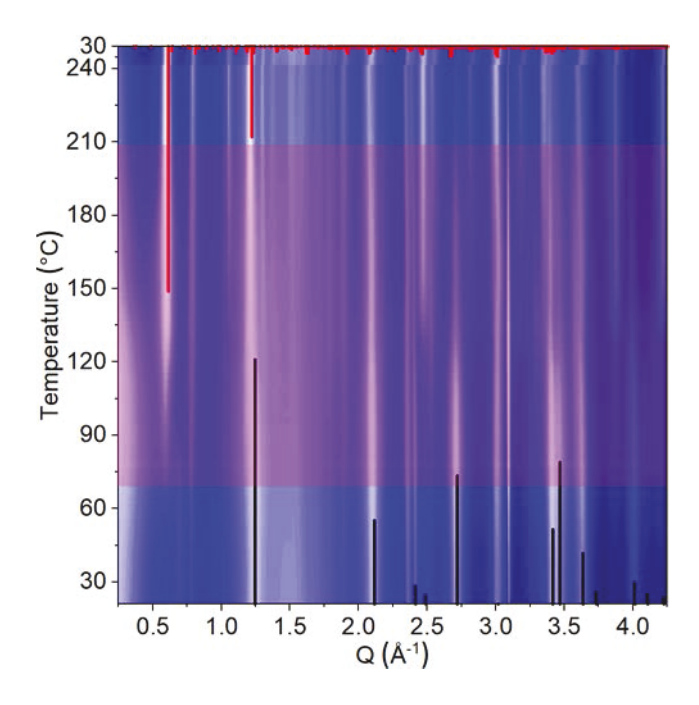


**Figure 2.** Contour plot of *in situ* synchrotron PXRD data. Each horizontal line is a PXRD pattern. Color mapping indicates peak intensity from blue to white. The purple highlighted box indicates a region where mackinawite peaks (black ticks) diminish with concurrent growth of  $[Fe_8S_{10}]Fe(en)_3 \cdot en_{0.5}$  peaks (red ticks).

The aforementioned *in situ* solvothermal setup is not suited to obtain quantitative data but rather provide a qualitative representation of the processes. A major challenge with replicating solvothermal methods for *in situ* PXRD studies is a significant concentration gradient within the sample in a vertically oriented capillary. Furthermore, there is significant sample movement throughout the measurement due to bubbles formed during solvent boiling. An average sample profile was collected by scanning across the solvent-sample interface, but in our experience this is not sufficient for precise quantification of phase fractions. The *in situ* synchrotron PXRD experiment provides clear evidence for a transition of mackinawite into [Fe<sub>8</sub>S<sub>10</sub>]Fe(en)<sub>3</sub>·en<sub>0.5</sub> and no significant changes to the overall hexagonal Fe<sub>1-x</sub>S and elemental Fe content were observed.

To ensure elemental Fe or hexagonal Fe<sub>1-x</sub>S are not required to transform mackinawite into intercalated [Fe<sub>8</sub>S<sub>10</sub>]Fe(en)<sub>3</sub>·en<sub>0.5</sub>, several control experiments were performed. First, a strong permanent magnet was used to mechanically remove elemental Fe, resulting in a sample of mackinawite (~62% wt.) with hexagonal Fe<sub>1-x</sub>S as the only detectable crystalline impurity (**Figure S4**). Once again, the transition from mackinawite to [Fe<sub>8</sub>S<sub>10</sub>]Fe(en)<sub>3</sub>·en<sub>0.5</sub> was reproduced successfully in a laboratory experiment (**Figure S5**). Second, a sample of single-phase hexagonal Fe<sub>1-x</sub>S was reacted with ethylenediamine in the presence of NH<sub>4</sub>Cl for 3 days at identical solvothermal conditions and no changes in the starting Fe<sub>1-x</sub>S were found (**Figure S5**). Thus, the only component which is chemically modified by the reaction with ethylenediamine and the only source of Fe for chelating tris-en complexes is mackinawite.

As depicted in **Figure 3**, we propose that solvothermal treatment of mackinawite allows ethylenediamine to not only intercalate the Fe-S layers but also create intralayer Fe vacancies. Ethylenediamine's strong affinity to chelate Fe results in penetration of the tetragonal FeS layers to bond with Fe, producing stable [Fe(en)<sub>3</sub>]<sup>2+</sup> cations. Starting from an Fe<sub>10</sub>S<sub>10</sub> layer, two Fe atoms must be leached, forming an [Fe<sub>8</sub>S<sub>10</sub>]<sup>2-</sup> layer and two [Fe(en)<sub>3</sub>]<sup>2+</sup> cations. One cation, along with uncoordinated ethylenediamine, pack the interlayer space producing [Fe<sub>8</sub>S<sub>10</sub>]Fe(en)<sub>3</sub>·en<sub>0.5</sub>, while the remaining [Fe(en)<sub>3</sub>]<sup>2+</sup> is presumed to stay in solution and ultimately crystallize as the byproduct Fe(en)<sub>3</sub>Cl<sub>2</sub>. The process results in an oxidation of the intralayer Fe because the average oxidation state is changing from +2 in the neutral FeS layer of mackinawite to +2.25 in the negatively charged layer of [Fe<sub>8</sub>S<sub>10</sub>]<sup>2-</sup>. The conversion of FeS to [Fe<sub>8</sub>S<sub>10</sub>]Fe(en)<sub>3</sub>·en<sub>0.5</sub> was reproduced with handling chemicals and solvents and loading and opening autoclaves in the Ar-filled glovebox under air-free conditions, thus excluding oxygen as oxidizer. Ethylenediamine is known to exhibit substantial red/ox activity in the solvothermal synthesis of metal chalcogenides, <sup>16, 27</sup> and we

hypothesize that ethylenediamine get reduced upon oxidation of Fe in the transformation of FeS into [Fe<sub>8</sub>S<sub>10</sub>]Fe(en)<sub>3</sub>·en<sub>0.5</sub>.

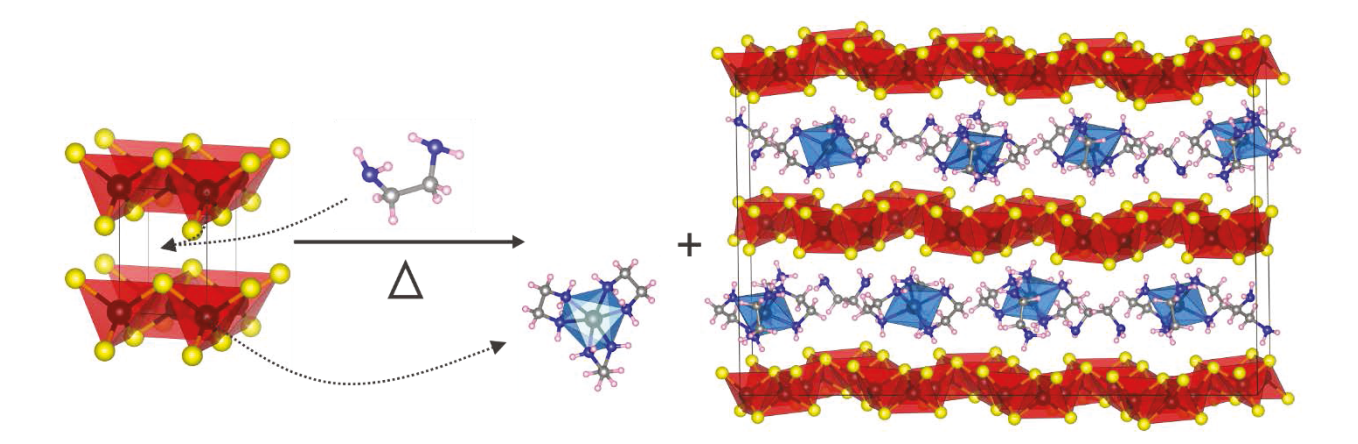


**Figure 3.** Schematic of transition from FeS, mackinawite, to [Fe<sub>8</sub>S<sub>10</sub>]Fe(en)<sub>3</sub>·en<sub>0.5</sub> under solvothermal conditions in ethylenediamine.

### **CONCLUSIONS**

Our findings highlight several important aspects of the diamine intercalation chemistry. Besides the commonly assumed intercalation of the neutral diamine molecules, the chemical reaction with Fe-Ch layers can result in Fe vacancy formation. In addition, diamines tend to coordinate the leached Fe, forming a second type of the intercalated species, positively charged chelating complexes, which can coexist with neutral diamine molecules in the interlayer space. Finally, we have recently shown that anions, such as chloride or bromide, may also be present in the interlayer space of complex layered Fe chalcogenides. Considering all the structural complexity one should use caution with deriving any conclusions regarding the composition, structure of Fe-Ch layer or intercalate, or their correlation to properties based on routine PXRD patterns, which only provide information regarding the interlayer spacing. To illustrate this point,

three calculated powder patterns are plotted in **Figure 4**, with an experimental high-resolution synchrotron PXRD pattern [Fe<sub>8</sub>S<sub>10</sub>]Fe(en)<sub>3</sub>·en<sub>0.5</sub> for comparison. One can see that removal of either Fe or all ethylenediamine species from the interlayer space only slightly affects the idealized PXRD patterns. On top of that, potential stacking defects and imperfections due to compositional gradients may produce misleading results of Rietveld refinement. Although the rich chemistry of diamine intercalation can add complexity, that inherent complexity opens a multitude of pathways to modify the composition, structure, and properties of intercalated phases via soft chemical methods.

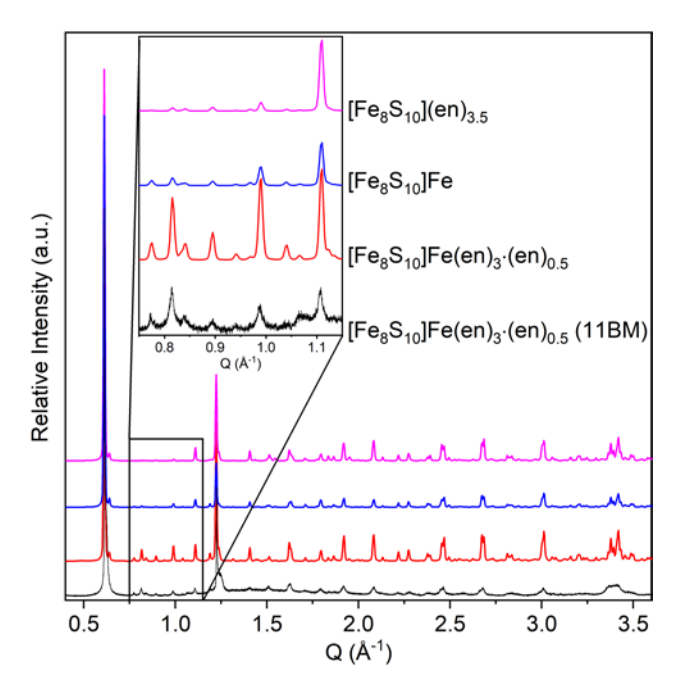


**Figure 4.** High resolution synchrotron PXRD pattern (black) plotted against its calculated pattern  $[Fe_8S_{10}]Fe(en)_3 \cdot en_{0.5}$  (red) and hypothetical patterns with all ethylenediamine removed (blue) and all interlayer Fe removed (magenta) from  $[Fe_8S_{10}]Fe(en)_3 \cdot en_{0.5}$ . Inset highlights the Q region (9.0 Å  $\geq d \geq 5.7$ ) with the most pronounced differences.

### ASSOCIATED CONTENT

### **Supporting Information.**

Details of synthesis and characterization procedures, crystallographic file for [Fe<sub>8</sub>S<sub>10</sub>]Fe(en)<sub>3</sub>·en<sub>0.5</sub>, additional X-ray diffraction refinement figures, magnetic data, and UV-

Vis-NIR Tauc plot for [Fe<sub>8</sub>S<sub>10</sub>]Fe(en)<sub>3</sub>·en<sub>0.5</sub>. This material is available free of charge via the Internet at <a href="http://pubs.acs.org">http://pubs.acs.org</a>.

### **AUTHOR INFORMATION**

# **Corresponding Author**

Dr. Kirill Kovnir, kovnir@iastate.edu

### **Author Contributions**

The manuscript was written through contributions of all authors.

### **Conflict of Interests**

Authors declare no conflict of interests.

# **Funding Sources**

This research was supported by National Science Foundation DMR-2003783 grant. Use of the Advanced Photon Source, an Office of Science User Facility operated for the U.S. Department of Energy (DOE) Office of Science by Argonne National Laboratory, was supported by the U.S. DOE under Contract No. DE-AC02-06CH11357.

### **ACKNOWLEDGMENTS**

The authors are thankful to Dr. J.V. Zaikina (ISU) for the access to UV-Vis-NIR spectrometer, and Dr. W. Xu, Dr. A. Yakovenko, and Dr. S. Lapidus (APS ANL) for help with collecting *insitu* and high-resolution synchrotron XRD patterns.

#### REFERENCES

- 1. Hsu, F. C.; Luo, J. Y.; Yeh, K. W.; Chen, T. K.; Huang, T. W.; Wu, P. M.; Lee, Y. C.; Huang, Y. L.; Chu, Y. Y.; Yan, D. C.; Wu, M. K., Superconductivity in the PbO-type structure alpha-FeSe. *Proc. Natl. Acad. Sci. U. S. A.* **2008**, *105* (38), 14262-14264.
- 2. Lai, X.; Zhang, H.; Wang, Y.; Wang, X.; Zhang, X.; Lin, J.; Huang, F., Observation of Superconductivity in Tetragonal FeS. *J. Am. Chem. Soc.* **2015**, *137* (32), 10148-10151.
- 3. Greenfield, J. T.; Kamali, S.; Lee, K.; Kovnir, K., A Solution for Solution-Produced β-FeSe: Elucidating and Overcoming Factors that Prevent Superconductivity. *Chem. Mater.* **2015**, 27 (2), 588-596.
- 4. Borg, C. K. H.; Zhou, X. Q.; Eckberg, C.; Campbell, D. J.; Saha, S. R.; Paglione, J.; Rodriguez, E. E., Strong anisotropy in nearly ideal tetrahedral superconducting FeS single crystals. *Phys. Rev. B* **2016**, *93* (9), 094522.
- 5. Vivanco, H. K.; Rodriguez, E. E., The intercalation chemistry of layered iron chalcogenide superconductors. *J. Solid State Chem.* **2016**, *242*, 3-21.

- 6. Pachmayr, U.; Nitsche, F.; Luetkens, H.; Kamusella, S.; Bruckner, F.; Sarkar, R.; Klauss, H. H.; Johrendt, D., Coexistence of 3d-ferromagnetism and superconductivity in [(Li1-x Fex )OH](Fe1-y Liy )Se. *Angew. Chem. Int. Ed. Engl.* **2015**, *54* (1), 293-297.
- 7. Burrard-Lucas, M.; Free, D. G.; Sedlmaier, S. J.; Wright, J. D.; Cassidy, S. J.; Hara, Y.; Corkett, A. J.; Lancaster, T.; Baker, P. J.; Blundell, S. J.; Clarke, S. J., Enhancement of the superconducting transition temperature of FeSe by intercalation of a molecular spacer layer. *Nat. Mater.* **2013**, *12* (1), 15-19.
- 8. Hosono, S.; Noji, T.; Hatakeda, T.; Kawamata, T.; Kato, M.; Koike, Y., New Intercalation Superconductor Lix(C6H16N2)yFe2–zSe2 with a Very Large Interlayer-Spacing and Tc = 38 K. *J. Phys. Soc. Japan* **2014**, *83* (11), 113704.
- 9. Xu, H. S.; Wang, X. X.; Gao, Z.; Huang, H. L.; Long, Y. Z.; Lu, Y. L.; Tang, K. B., New alkali-metal and 1,2-Diaminopropane intercalated superconductor Li (C3H10N2) Fe2Se2 with Tc = 45 K. *J. Alloys Compd.* **2018**, *735*, 2053-2057.
- 10. Hatakeda, T.; Noji, T.; Kawamata, T.; Kato, M.; Koike, Y., New Li-Ethylenediamine-Intercalated Superconductor Lix(C2H8N2)yFe2-zSe2 with Tc = 45 K. *J. Phys. Soc. Japan* **2013**, 82 (12), 123705.
- 11. Sedlmaier, S. J.; Cassidy, S. J.; Morris, R. G.; Drakopoulos, M.; Reinhard, C.; Moorhouse, S. J.; O'Hare, D.; Manuel, P.; Khalyavin, D.; Clarke, S. J., Ammonia-rich high-temperature superconducting intercalates of iron selenide revealed through time-resolved in situ X-ray and neutron diffraction. *J. Am. Chem. Soc.* **2014**, *136* (2), 630-633.
- 12. Shylin, S. I.; Ksenofontov, V.; Sedlmaier, S. J.; Clarke, S. J.; Cassidy, S. J.; Wortmann, G.; Medvedev, S. A.; Felser, C., Intercalation effect on hyperfine parameters of Fe in FeSe superconductor with  $T_c = 42 \, \text{K}$ . *EPL* **2015**, *109* (6), 67004.
- 13. Sun, H.; Woodruff, D. N.; Cassidy, S. J.; Allcroft, G. M.; Sedlmaier, S. J.; Thompson, A. L.; Bingham, P. A.; Forder, S. D.; Cartenet, S.; Mary, N.; Ramos, S.; Foronda, F. R.; Williams, B. H.; Li, X.; Blundell, S. J.; Clarke, S. J., Soft chemical control of superconductivity in lithium iron selenide hydroxides Li(1-x)Fe(x)(OH)Fe(1-y)Se. *Inorg. Chem.* **2015**, *54* (4), 1958-1564.
- 14. Wu, D.; Guo, Z.; Liu, N.; Zhou, L.; Mao, Y.; Wan, L.; Sun, F.; Yuan, W., A new intercalated iron sulfide (C2H8N2)0.4Fe2S2 from solvothermal route: Synthesis, structure and tunable magnetism. *Inorg. Chem. Commun.* **2018**, *91*, 72-76.
- 15. Stahl, J.; Shlaen, E.; Singer, H.; Johrendt, D., Systematic dimensional reduction of the layered beta-FeSe structure by solvothermal synthesis. *Dalton Trans.* **2018**, *47* (10), 3264-3271.
- 16. Gamage, E. H.; Greenfield, J. T.; Unger, C.; Kamali, S.; Clark, J. K.; Harmer, C. P.; Luo, L.; Wang, J.; Shatruk, M.; Kovnir, K., Tuning Fe-Se Tetrahedral Frameworks by a Combination of [Fe(en)3](2+) Cations and Cl(-) Anions. *Inorg. Chem.* **2020**, *59* (18), 13353-13363.
- 17. Pak, C.; Kamali, S.; Pham, J.; Lee, K.; Greenfield, J. T.; Kovnir, K., Chemical excision of tetrahedral FeSe(2) chains from the superconductor FeSe: synthesis, crystal structure, and magnetism of Fe(3)Se(4)(en)(2). *J. Am. Chem. Soc.* **2013**, *135* (51), 19111-19114.
- 18. Wu, M.; Rhee, J.; Emge, T. J.; Yao, H.; Cheng, J. H.; Thiagarajan, S.; Croft, M.; Yang, R.; Li, J., A low band gap iron sulfide hybrid semiconductor with unique 2D [Fe(16)S(20)](8-) layer and reduced thermal conductivity. *Chem. Commun.* **2010**, *46* (10), 1649-1651.

- 19. Halcrow, M. A., *Spin-crossover materials: properties and applications*. Wiley & Sons: Oxford, UK, 2013.
- 20. Lei, H. C.; Abeykoon, M.; Bozin, E. S.; Petrovic, C., Spin-glass behavior of semiconducting K<sub>x</sub>Fe<sub>2-y</sub>S<sub>2</sub>. *Phys. Rev. B* **2011**, *83* (18), 180503.
- 21. Shoemaker, D. P.; Chung, D. Y.; Claus, H.; Francisco, M. C.; Avci, S.; Llobet, A.; Kanatzidis, M. G., Phase relations in K<sub>x</sub>Fe<sub>2-y</sub>Se<sub>2</sub> and the structure of superconducting K<sub>x</sub>Fe<sub>2</sub>Se<sub>2</sub> via high-resolution synchrotron diffraction. *Phys. Rev. B* **2012**, *86* (18), 184511.
- 22. Zavalij, P.; Bao, W.; Wang, X. F.; Ying, J. J.; Chen, X. H.; Wang, D. M.; He, J. B.; Wang, X. Q.; Chen, G. F.; Hsieh, P. Y.; Huang, Q.; Green, M. A., Structure of vacancy-ordered single-crystalline superconducting potassium iron selenide. *Phys. Rev. B* **2011**, *83* (13), 132509.
- 23. Lei, H.; Abeykoon, M.; Bozin, E. S.; Wang, K.; Warren, J. B.; Petrovic, C., Phase diagram of K(x)Fe(2-y)Se(2-z)S(z) and the suppression of its superconducting state by an Fe2-Se/S tetrahedron distortion. *Phys. Rev. Lett.* **2011**, *107* (13), 137002.
- 24. Tsuchiya, Y.; Ikeda, S.; Kobayashi, H., Fe-57 Mossbauer spectroscopic studies of single-crystalline KxFe2-yS2 and KxFe2-ySe2. *Hyperfine Interact.* **2016**, *237*, 44.
- 25. Ksenofontov, V.; Wortmann, G.; Medvedev, S. A.; Tsurkan, V.; Deisenhofer, J.; Loidl, A.; Felser, C., Phase separation in superconducting and antiferromagnetic Rb0.8Fe1.6Se2 probed by Mossbauer spectroscopy. *Phys. Rev. B* **2011**, *84* (18), 180508.
- 26. Texier, Y.; Deisenhofer, J.; Tsurkan, V.; Loidl, A.; Inosov, D. S.; Friemel, G.; Bobroff, J., NMR study in the iron-selenide Rb0.74Fe1.6Se2: determination of the superconducting phase as iron vacancy-free Rb0.3Fe2Se2. *Phys. Rev. Lett.* **2012**, *108* (23), 237002.
- 27. Li, J.; Chen, Z.; Wang, R. J.; Proserpio, D. M. Low Temperature Route towards New Materials: Solvothermal Synthesis of Metal Chalcogenides in Ethylenediamine. *Coord. Chem. Rev.* **1999**, *190–192*, 707-735.

For Table of Contents Only

